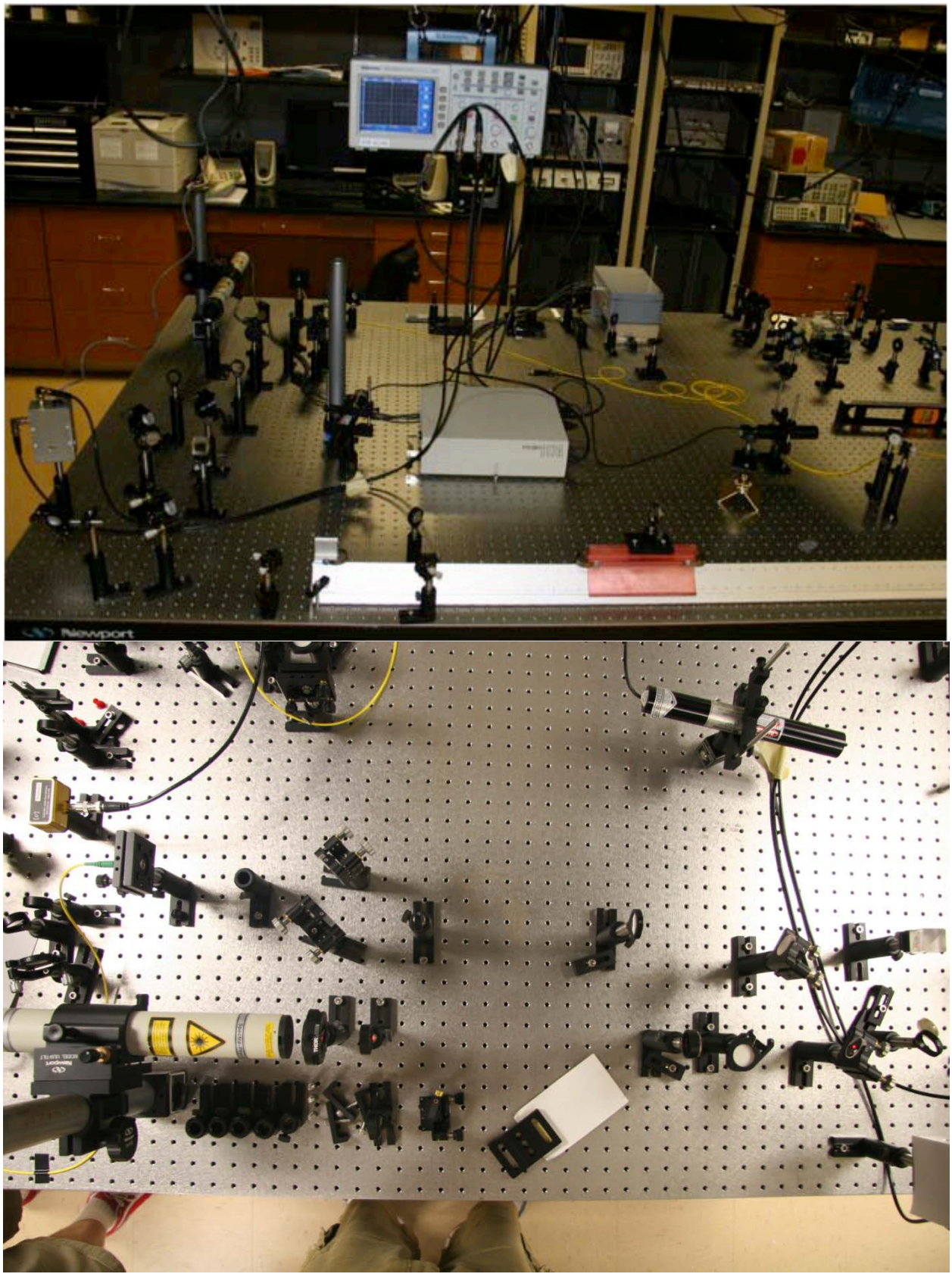

The wavemeter set-up. Top: Scope, air track and stabilized HeNe. Bottom: top view of HeNe polarizer and lens system.

Diode Lasers for Rubidium Spectroscopy

J. Johnson, B. Clark, and J. Seaberg
Bethel University
St. Paul, MN 55112
(Dated: May 14, 2010)

It is demonstrated that a home-built, external-cavity laser diode system can produce continuous, stable wavelength tunability, sufficient for Doppler-broadened spectroscopy of rubidium vapor. It is also shown that hyperfine structures can be resolved simply from back-reflection off of the windows of the rubidium cell. Experimentally observed spectra were successfully matched with their respective resonance frequencies via the observation of hyperfine features. Quantitative analysis of the spectra was successful in estimating the frequency difference between resonance frequencies within 0.1 GHz.

PACS numbers:

INTRODUCTION

The use of diode lasers in atomic spectroscopy is a common practice today. Nevertheless, it is a valuable technique for the study of atomic energy levels, with the capability to resolve hyperfine structures. Moreover, it represents a unique opportunity to learn about several areas of physics, intersecting the disciplines of optics and atomic physics. This paper presents an undergraduate study of rubidium spectroscopy, done with a home-built external cavity diode laser (ECDL). We first outline the concepts and theories underlying the operation and characteristics of the laser diode and absorption spectroscopy. In each case the general theory is presented along with the specifics of our experiment. We then give our results in terms of absorption peaks correlating to the appropriate atomic transitions. More figures relevant to spectroscopy data and laser characteristics are included in the results section.

The ultimate goal of the project was to obtain spectral data of Rb absorption peaks around 780 nm, and then match these peaks with known atomic transitions in Rb. However, an intermediate and antecedent goal was the construction of the external cavity diode laser, capable of producing these resonances in the Rb vapor. We desired to demonstrate the tuning capability of our laser across the frequency of the known atomic transitions of rubidium.

DIODE LASER

Diode lasers are increasingly being used in many atomic and optical physics experiments, particularly in the undergraduate laboratory. These lasers provide coherent light and have reasonable output power, high electrical to optical efficiency, continuous wavelength tunability and are relatively small and low cost [1]. For these reasons, they are particularly appealing for atomic physics. Because, however, these bare diodes have a large linewidth (50-100 MHz) and a majority of experiments need linewidths less than 1MHz, diode lasers have been manipulated and studied in order to optimize their frequency stability and absolute frequency. These diodes are also extremely sensitive to optical feedback (as little as 10^{-6} of the output light fed back can affect its frequency stability). In order to significantly reduce the bandwidth of a diode laser, an external or extended cavity that has frequency selecting optical elements is usually needed.

A cutaway view of the Sharp 780 nm diode laser, LT025MD0, that we used for our experiment is shown in Figure 1 [2]. The actual semiconductor device is an LD chip bonded to a heat-sink, in which wires are connected to the outside of the housing. While most of the light is emitted through the front facet, a fraction still comes out the back facet. The main beam, out of the front facet, is elliptical and strongly diverging. A closer view of a typical laser diode is shown in Figure 2. Current is driven through the chip from top to bottom, which creates electron-hole pairs that recombine in the active layer, and light is emitted in the process. The light is confined in the chip to a narrow channel (about 2 microns high, 10 microns wide, and 400 microns long), shown as a wavy line in Figure 2. At the ends of the channel are the facets of the chip, which act as partially reflecting mirrors that enclose the laser cavity [2].

When a laser is being injected with low levels of current, the optical losses are greater than the gain and population inversion is not achieved. The light output is therefore broad-band, spontaneous emission. When the current is above a threshold current, however, a coherent beam is emitted that increases linearly with injection current. Laser diodes are generally very efficient compared to other sources of laser light, outputting power in coherent radiation as high as fifty percent of the input electrical power [2]. Frequency of a laser is also a function of temperature, so as the temperature is increased, the wavelength of the laser increases. A power versus current plot of our stabilized Sharp 780 diode at both 12.7 and 20 degrees Celsius is shown in Figure 3.

The diode laser housing and lens collimation set-up

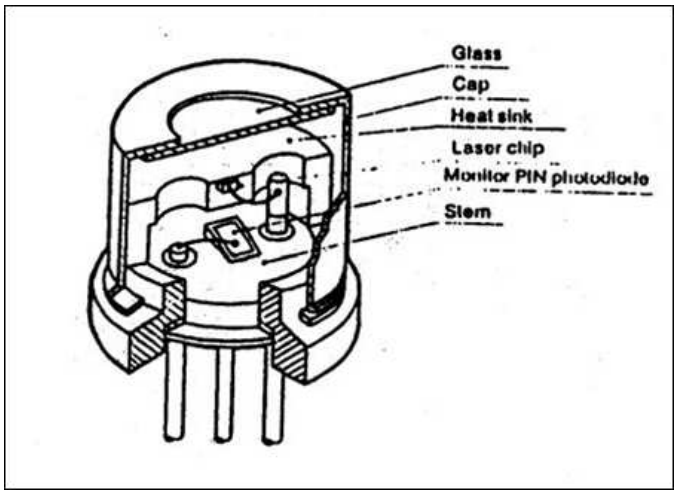

FIG. 1: Cutaway view of Sharp 780 nm laser diode where the chip is mounted. The glass window, cap, heat sink, laser chip, and stem positions are shown. Semiconductor physics determine the behavior of the p-n junction in the Laser chip, which has PIN connections that connect the laser chip outside of the housing. J. Swihart,Indiana Advanced Laboratories (2009).

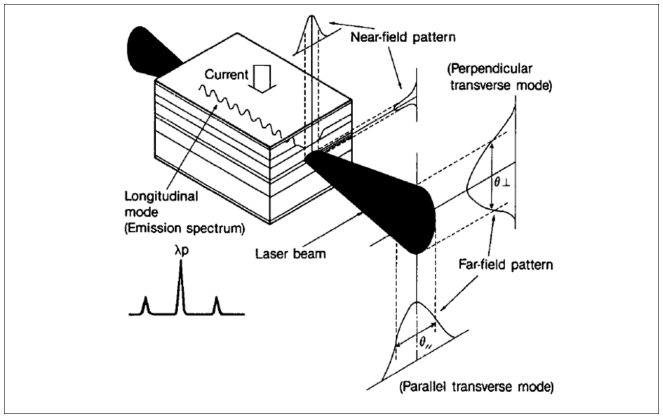

FIG. 2: Close-up schematic view of a laser diode chip. The current is driven from top to bottom through the chip. Electron-hole pairs are created and recombined in the active layer, emitting light that is confined in a narrow channel in the chip. The facets at the ends act as partially reflecting mirrors enclosing the cavity. K. Libbrecht, Caltech Advanced Atomic and Optical Physics Laboratory,1-7 (2010).

used is modeled after the external cavity design used at the National Institute of Standards and Technology (NIST) in Boulder, Colorado. A schematic of the diode housing is shown in Figure 3. A protection circuit is incorporated in order to remove current transients and protect from static discharge or back-currents [3]. A thermistor monitors the temperature of a diode housing that is thermally isolated from any other elements. The thermistor is read by a commercial temperature control source, which controls a Peltier thermoelectric cooler at

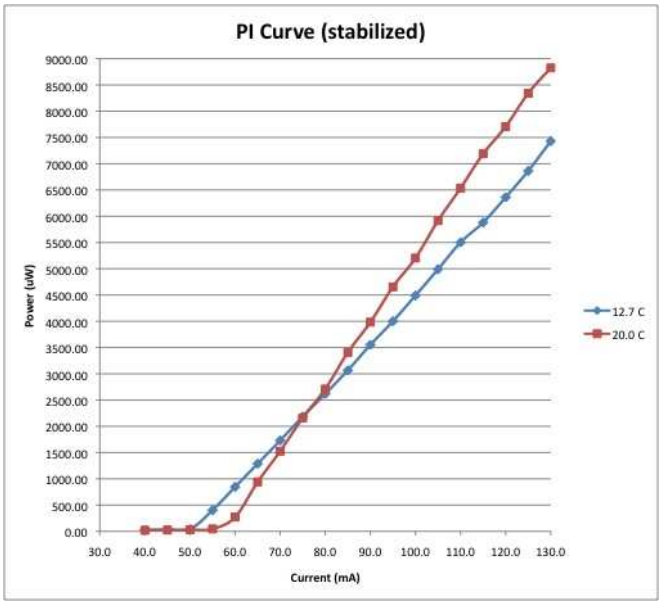

FIG. 3: Plot of power versus current of the Sharp 780 nm diode. When the current is above threshold, the laser emits a coherent beam, which increases in intensity linearly with injection current. The power is also increased with increasing temperature, shown by the power of both 12.7 and 20 degree Celsius temperatures.

the base of this housing so that the temperature of the diode is constant and known. The alignment of the collimating lens is of particular importance; therefore, a separate housing with fine adjustment capabilities is incorporated. This housing contains two concentric, slip-fit, adjustments that are slightly offset so that the collimation of the beam can be optimized. There is an additional screw on the diode housing that finely adjusts the distance that the lens is from the face of the diode, which is denoted the Z-direction adjustment. Optimal positioning requires that the diode be at the focal length of the lens. A piezo-electric transducer (PZT) is secured between the grating and its mount, which is used to modify the cavity length for fine frequency tuning [3]. The diode housing then sits on a copper plate, which serves as a heat sink. The entire set up is enclosed in an aluminum, covered box that shields the laser from air currents, dampens acoustic vibrations, and improves temperature stability.

External Cavity Stabilization

For the rubidium spectroscopy experiment described, we have used the Littrow configuration, shown in Figure 4. In this set-up, the first-order beam diffracted from the grating is coupled back into the diode and the zeroeth-order light, directly reflected, forms the output beam. This configuration increases the output power while also reducing feedback, thus, overall improving ef-

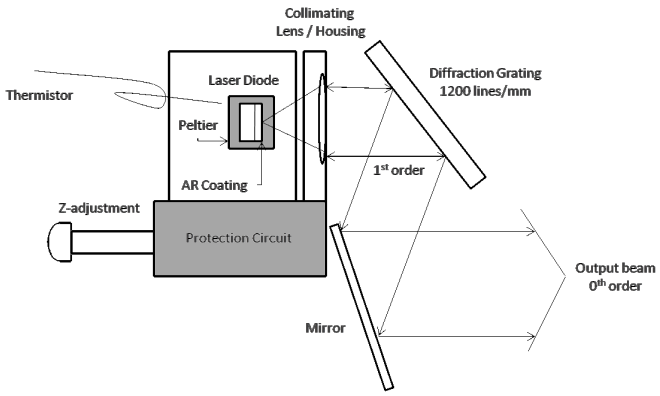

FIG. 4: Schematic of laser diode housing and external cavity. The Littrow configuration is used, in which the first-order is reflected off of a grating back into the diode, while the zeroeth-order is reflected off of a mirror and is then used as the output beam. A protection circuit, temperature control components, and a PZT are incorporated for added control, stability, and tunability.

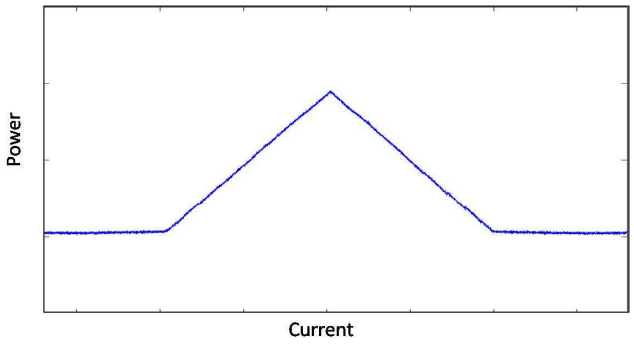

FIG. 5: A scope-view of the hats method of stabilization is shown. When the current is above threshold, signal representing the power of the diode takes on a triangular shape. The broader that the base of the triangles are, the more quickly the laser gets off of the threshold current, and the more stable the laser is. Both the vertical and z-components are used to optimize the stability in this way.

ficiency. When the first order is reflected back into the diode, the linewidth is significantly reduced to less than 1MHz, and by adjusting the grating angle, the lasing wavelength can be selected. A drawback, however, from this configuration is that the output beam is wavelength dependent which leads to alignment problems while tuning the laser.

Originally, we used a 2400 line/mm grating which was blazed for visible light in order to take advantage of a larger grating angle and more convenient reflection of the zeroeth-order output beam, determined by the Grating Equation found in Equation 1, where a is the spacing between grating slits, calculated as $a = \frac{1}{1200\ lines/mm * 1000\ mm/m}$.

$$2asin(\theta) = m\lambda \tag{1}$$

The grating angle for the first-order of 780 nm light incident on a 2400 lines/mm grating to be coupled back into the diode in Littrow configuration, therefore, is about 69.4 degrees, and 27.9 degrees for 1200 lines/mm. We had significant trouble using either the 2400 or 1200 lines/mm gratings that were blazed for visible light. When first stabilizing a diode, we aligned the grating by eye so that the first-order was approximately reflected back into the diode. Then, using a photodetector, we monitored the power of the zeroeth order while systematically adjusting the grating. Evidence of stabilization using this method includes an overall increase in power of the zeroeth order (where we ultimately try to obtain the maximum power possible) and jumps in the power of this beam, which are evidence of the laser changing between modes.

A second method of stabilization, which we have called the hats method, is then implemented. We reduce the current of the diode so that it is near threshold and modulate the current by connecting a frequency generator to the current source. We modulate the current with a triangle wave of frequency 320 Hertz and a peak-to-peak voltage of 100mV. We can then view the power of the zeroeth order as seen in Figure 5. The section of the figure that resembles a triangle is representative of when the diode is lasing above threshold, while the sections that resemble a DC voltage show when the laser is operating below threshold. By adjusting the vertical component of the grating and the Z-component of the lens housing, we can optimize the stabilization of the diode. This is visualized by making the base of the triangle sections as wide as possible, which indicates the laser getting off of threshold quickly. By reducing the current, more precise adjustments of the hats can be made.

A laser diode contains four main properties of interest when considering tunability. The first is the medium gain, which depends on the properties of the semiconductor material that the laser is made of. This gain is a broad peak, and it's position is mainly dependent on temperature. It is useful to set the desired lasing wavelength in the center of the medium gain in order to optimize the power and stability of the lasing frequency. Secondly, the internal cavity of the diode junction forms a small optical cavity, like a Fabry-Perot etalon. The net gain of this cavity is frequency-dependent and periodic in frequency. The period of this is the *free spectral range* ($\Delta\nu_{FSR} = c/2Ln$) and the cavity gain function will shift in frequency when the temperature or current of the diode is changed. Typically, this shift is 3MHz/μA for a fixed temperature. A third property that effects diode tuning is the grating feedback. Gratings disperse light, so only light from a narrow wavelength band is fed back into a laser for a fixed, horizontal grating angle. The spectral width of the grating feedback, therefore, can be

approximated by $\nu/\Delta\nu = N$, where ν is frequency and N is the number of grating lines. In our set-up, for example, we have about a 0.1-cm wide laser beam, so for a 25 mm, 1200 line/mm grating and a 780 nm laser, the spectral width is about 320 GHz. Finally, similar conceptually to the internal cavity, the external cavity formed between the grating and the laser cavity plays a role in tuning. Since the external cavity is much larger than the internal, however, the curve shifts by moving the grating position with the PZT [4].

Tuning

Then, by observing the tunability of the laser, we can further diagnose stability. For this, we use an Ocean Optics optical fiber, spectrometer and Spectra Suite software, which is precise to about 0.5 nm. By adjusting the horizontal component of the grating, we can adjust the frequency of the laser and view the diode tune on the Spectra Suite program. While using both of the gratings that were blazed for visible light, we had difficulty obtaining more than 1 or 2 mW of power from the first order. Being that Sharp 780 diodes operate at around 40 mW, our output beam was significantly reduced. In order to make wavelength measurements, at least 1 mW is needed, and because of loss in optical elements such as the optical isolator, mirrors, and lenses, this was not possible. In addition, the signal from the zeroeth order seemed to contain significant noise during the initial photodetector and hats stabilizations and we had much difficulty tuning the frequency of the laser. We experienced instability and inconsistency in the frequencies selected during tuning. We hypothesized that this was due to the fact that the gratings were blazed for visible light, whereas we were working with a near infrared source. An additional conclusion was that because, at most, 2 mW was emitted in the zeroeth order, a considerable fraction of the remaining power was being reflected back into the diode. Though diodes have an anti-reflection coating on the face to reduce the effects of feedback, diode lasers are still very sensitive to feedback, so when a significant amount of the lasers power is being fed back it can interfere with stabilization and tunability.

After experiencing instability with both gratings blazed for visible light, we tried a third 1200 lines/mm Edmund Optics grating blazed for 750 nm. Without feeding back the first-order, we obtained about 15 mW in the first-order and 5 mW in the zeroeth order. We then stabilized and optimized the laser using the above techniques, and obtained approximately 8 mW in the zeroeth order, an improvement of about 7 mW from the gratings blazed for visible light. We observed a reasonable increase in the power of the laser when stabilized and no longer detected feedback. Further, we were able to tune over a 9 nm range using the grating alone. This tuning is depicted in Figure 6.

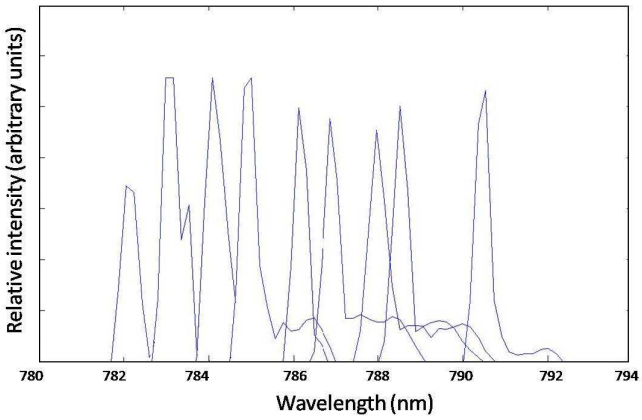

FIG. 6: Coarse tuning of the Sharp 780 nm diode laser using only a grating. We scanned approximately 9 nm by frequency selection using feedback from the first-order.

ABSORPTION SPECTROSCOPY

The physics of the laser diode aside, spectroscopy plays an essential role in our understanding of the structure of atoms and molecules. In fact, much of what we know about the structural nature of atomic matter comes from spectroscopic investigations. Through the absorption and emission spectra that are emitted when electromagnetic radiation interacts with matter we can understand the way that the components of molecules and atoms interact [5]. Before detailing our setup and results, it is important to develop a basic understanding of what takes place on the atomic level when light is absorbed by atoms. We examine the case of rubidium in particular.

Absorption and Emission of Photons

The component of the atom that is most closely tied to the emission and absorption of radiant energy is the bound charge, electrons that are contained within atoms (as opposed to free electrons). The electrons form a cloud around the nucleus of the atom which is composed of various levels. If an atom is in its ground state configuration, the electrons fill all the lowest possible energy levels. However, if an atom experiences an increase in energy, the electrons will move to higher energy levels, causing the atom to be in its excited state. The excited state is a condition that is temporary, as the electrons will eventually return to their lower energy levels [6].

As electrons move from higher energy levels to lower energy levels (and the atom moves from an excited state to ground state), the atom must release the energy in some form, which often times corresponds to the emis-

sion of a photon. Conversely, the absorption of a photon can cause an atom to move into an excited state. These processes are pictured in Figure 7. The latter is the case in absorption spectroscopy, the phenomenon we observe in this experiment. The emission of photons by atoms is actually regarded as the principal source of light in the universe. Because the electrons move from energy level to energy level in a seemingly instantaneous fashion, their movement is termed a quantum jump, as the difference in energy stored in the atom between the initial and final states can be quantized [6].

When an atom emits a photon, the energy of the photon is exactly equal to the decrease of energy in the atom. This change in energy, $\Delta\mathcal{E}$, is related to a particular frequency ν by way of the equation $\Delta\mathcal{E} = h\nu$. This light frequency is termed a resonant frequency of the atom. Each atom has different resonant frequencies at which it emits light. Furthermore, these resonant frequencies correspond to light that the atom can easily absorb, because of the correlation between the frequency ν and the quantum jump that the atom experiences. The resonant frequencies for a particular atom depend on the various ways in which the outer electrons of the atom can transition to higher energy levels. Each resonant frequency in turn corresponds to a particular wavelength. By examining the atomic structure of rubidium, we can correlate observed absorption spectra with specific resonant frequencies (and hence, wavelengths) of the electromagnetic radiation interacting with the matter [6].

It is important to note that the movement of electrons in atoms is far more complicated than the simplistic model outlined above, involving characteristics of the electrons such as electron spin and angular momentum, in addition to changing orbitals. For a more thorough treatment of these ideas, see [7]. A further characteristic of the atom that influences the energy of the atom is the nuclear spin. The influence of nuclear spin on the atomic structure of the atom is known as hyperfine structure. That is, hyperfine structure is due to nuclear spin and its interaction with other spins. In the absorption of a photon, the hyperfine structure of the atom can be observed in both the ground state and the excited state [8].

We now focus on the possible electron transitions of rubidium. There are two rubidium isotopes (85 and 87) whose different structures (and consequently different quantum jumps) allow for different resonance frequencies. Each of the isotopes have two hyperfine ground states whose resonance frequencies are spaced on the order of GHz. The hyperfine excited states are more narrowly spaced (the resonant frequencies are separated on the order of MHz) [9]. In both isotopes, the transitions observed at the 780-nm spectral line are of the form $5^2S_{1/2} \rightarrow 5^2P_{3/2}$ (see Figure 9). Due to our experimental setup, our spectra exhibit a phenomenon called Doppler broadening, which would normally prevent us from resolving the hyperfine features in the excited states. The hyperfine features of the ground states, because they are spaced by frequencies on the order of GHz, are easily resolved with our experimental setup, and we thus expect to see four resonance frequencies if both rubidium isotopes are present in the gas used in our setup (as seen in Figure 10) [8]. In order to resolve the hyperfine features of the excited states one must employ a technique called saturation spectroscopy.

The experimental setup for spectroscopy is shown in Figure 8. Saturation spectroscopy is generally conducted experimentally by directing a second laser through the gas in the opposite direction of the first. Though this was not an initial goal in our experimental setup, due to the reflection of the initial beam on the glass of the rubidium cell, we were able to produce saturation spectroscopy and thus observe the hyperfine structure of the excited state.

Doppler Broadening

Though theoretically each resonance frequency of rubidium corresponds to a particular natural linewidth, that is the width of frequency that corresponds to the quantum jump, the spectral dips produced by absorption spectroscopy are subject to the phenomenon of Doppler broadening. Because of doppler broadening, we do not observe a rigid frequency region over which absorption occurs, but rather a gradual dip that contains the resonance frequency (as can be seen in Figure 10).

The gradual dip stems from the fact that the gas atoms are moving with respect to the electromagnetic radiation. Assume that an excited atom is moving with velocity v relative to a stationary observer (located at the detector). Assuming the central resonant frequency for a given absorption line is ω_0, the apparent absorption frequency (due to the Doppler effect) is $\omega_a = \omega_0 + k \cdot v$, where k is the wave vector corresponding to the absorbed electromagnetic wave. Therefore, the observed absorption frequency ω_a is increased when $k \cdot v > 0$ (atoms moving in the same direction as the light is traveling) and decreased when $k \cdot v < 0$ (atoms moving in opposite direction of the light). Thus by way of Doppler broadening, we observe resonant frequencies over a continuous dip, in which lies the central resonant frequency ω_0 [5].

SPECTROSCOPY METHODOLOGY

In order to obtain higher precision wavelength measurements we utilized Bethel's Michelson wavemeter built by Sarah Anderson. The operation of the wavemeter is involved and will not be discussed here, but for a detailed description see [10]. Beam alignment within the wavemeter proved to be troublesome, since tuning with a Littrow configuration alters the beam direction. Af-

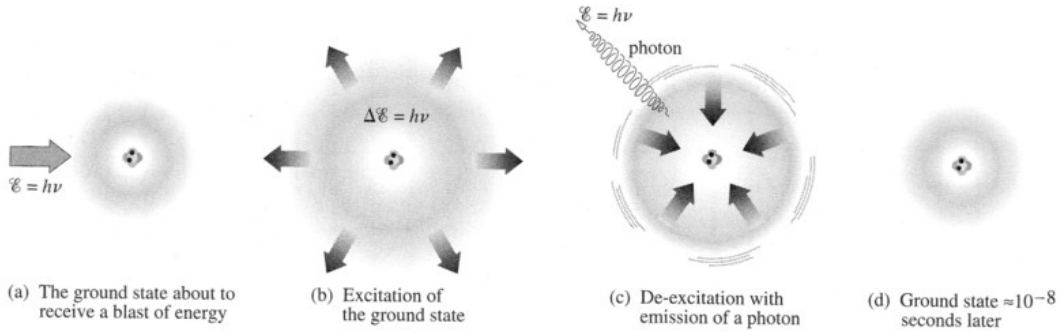

FIG. 7: The interaction of electromagnetic radiation with an atom. (a) Energy is approaching an atom in its ground state. (b) The energy is absorbed by the atom because it matches the required energy needed for the atom to reach an excited state and reach a higher energy level. (c) The atom loses the energy through the emission of a photon. (d) The atom returns to its ground state. E. Hecht, Optics, 4th ed., 64 (2002).

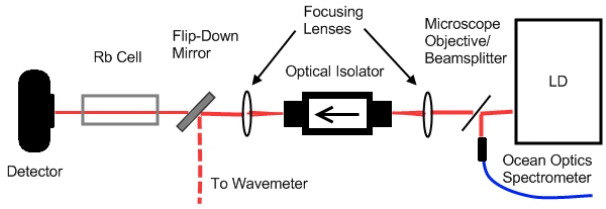

FIG. 8: Experimental setup for rubidium spectroscopy. An optical isolator is implemented to minimize unwanted feedback into the diode. A flip-down mirror allowed for rapid transitions between wavelength measurements and resonance scanning.

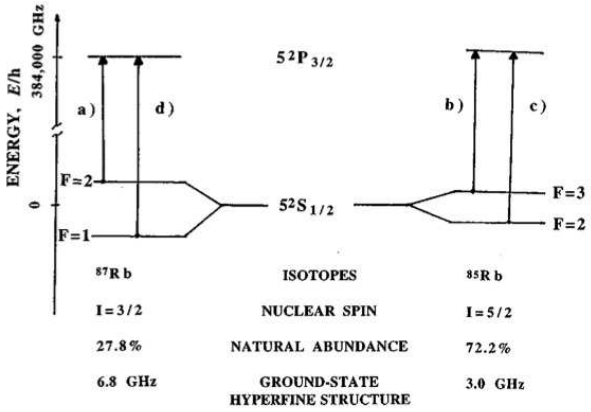

FIG. 9: A diagram depicting the energy levels for the 780-nm resonance transitions in rubidium. For both isotopes, the transition is $5^2S_{1/2} \rightarrow 5^2P_{3/2}$. The hyperfine splittings are depicted for the ground states of both isotopes as they can be resolved experimentally without the use of saturation spectroscopy. The hyperfine splittings for the excited states are omitted as they are not resolved without saturation spectroscopy. K. Razdan and D.A. Van Baak, American Journal of Physics **67**, 832-836 (1999).

ter realignment, however the wavemeter provided the picometer resolution needed to tune to the rubidium resonances. Even when stabilized, tuning of the LD was very sensitive, and subject to numerous mode hops. We found it helpful to use a combination of adjustments in grating angle, current, temperature and PZT offset to tune to the desired wavelength.

As detailed in the theory behind the diode laser, we employ a piezoelectric transducer (PZT) to scan the cavity length and consequently scan the range of optical frequencies in which lie the resonance frequencies of rubidium. In order to perform quantitative analysis of the spectrum, it was necessary to compute the range of frequencies scanned by the PZT. Using a function generator we programmed the PZT to scan over 120 volts, from 10 V to 130 V. According to the PZT specifications, the physical distance the PZT moves is $3\mu m$ per 200 volts (which is equivalent to 15 nm per volt). In order to relate change in optical frequency with the scanning of the PZT, we derive here the relationship between change in cavity length and change in optical frequency.

For a particular cavity mode q, we have the following expression for optical frequency:

$$\nu_q = \frac{qc}{2L}$$

where L is the cavity length. Taking the partial of ν_q with respect to L yields

$$\frac{\partial \nu_q}{\partial L} = -\frac{qc}{2L^2}.$$

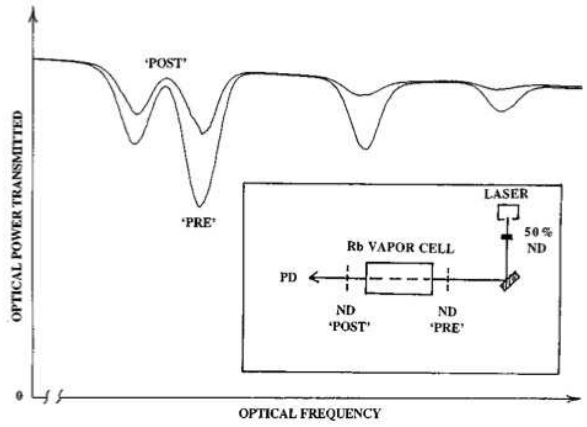

FIG. 10: The four Doppler broadened resonance frequencies for the 780-nm resonance transitions in rubidium. The horizontal axis represents a frequency range of approximately 10 GHz, and the frequencies pictured are on the order of 384,000 GHz. K. Razdan and D. A. Van Baak, American Journal of Physics **67**, 832-836 (1999).

Rearranging, we establish the following expression for the change in ν_q in terms of the change in cavity length:

$$\Delta\nu_q = -\frac{qc}{2L^2}\Delta L.$$

By taking account the θ of the diffraction grating (since the PZT drives the diffraction grating in the direction of the vector normal to the grating surface), we can rewrite the above equation as follows:

$$\frac{\Delta\nu_q}{V} = -\frac{qc}{2L^2}\frac{15 \text{ nm } cos\theta}{V}.$$

By definition,

$$\frac{q\lambda}{2} = L$$

thus

$$q = \frac{2L}{\lambda}.$$

Substituting this into our equation for $\frac{\Delta\nu_q}{V}$ yields

$$\frac{\Delta\nu_q}{V} = -\frac{c}{\lambda L}15 \text{ nm } cos\theta V$$

which after substituting the appropriate values for our experiment yields $\frac{\Delta\nu_q}{V} = -0.146$ GHz per V. This value is important in quantitatively analyzing the plots of the Rb spectra as it provides a way to convert from the volts we are scanning with the PZT to the optical frequency observed between resonance frequencies.

RESULTS

In order to adequately produce spectra near the 780-nm wavelength, it was important to properly tune the laser with the wavemeter, which calculates the wavelength of an unknown coherent light source through comparison to a known Helium-Neon source. The vacuum wavelength for the 780-nm transition in Rb is 780.241 nm [11]. Wavelength of light, however, is dependent on the matter it is propagating through, therefore we must take into account the specific conditions of the environment that the experiment is being conducted in. Our laboratory operated at about atmospheric pressure with a temperature of about 22 degrees Celsius and humidity of 29%. We used this information to calculate the index of refraction of specific wavelengths of light in these conditions using the NIST Metrology Toolbox [12]. We found the index of refraction of our laser to be n_{780nm} = 1.000268352, while the wavelength of the known HeNe laser was $n_{633\text{nm}}$ = 1.000269675. Therefore, $\frac{n_{780\text{nm}}}{n_{633\text{nm}}}$ = 0.999998677. We can multiply the vacuum wavelength of interest by this ratio to account for the index of refraction of the air in our lab, $780.241 \cdot \frac{n_{780\text{nm}}}{n_{633\text{nm}}}$ =780.242. In order to observe rubidium resonances, then, we needed to observe a wavelength of 780.242 nm on the wavemeter.

We recorded four successful wavelength measurements before proceeding with spectroscopy. After averaging these four measurements we obtained a mean wavelength of 780.242 nm with a standard deviation of 0.08 pm.

Upon the proper tuning of the laser, we sent the laser through the Rb cell and obtained the spectra pictured in Figures 11 and 12. The plots in these two Figures are separated by a mode hope. Because of the mode hop, we were unable to image all four resonant frequencies at the same time. Because our experimental setup did indeed produce saturation spectroscopy (albeit unintentionally), we were able to identify the four peaks due to their hyperfine features. The expected hyperfine features for each transition are pictured in Figures 13 and 14 which can be found in [13]. Figure 15 displays our experimental data for the first two of the four peaks and is included so that the reader can compare the hyperfine features in our plots to the expected hyperfine features found in [13] (see Figures 13 and 14). Finally, Figure 16 displays the observed spectra from our experiment combined together so that all four resonance frequencies are visible. This plot can be compared to Figure 10.

By utilizing the results for $\frac{\Delta\nu_q}{V}$ from the previous section we are able to estimate the optical frequency differences between resonance frequencies. However, due to the mode hop we could only observe two peaks at the same time, thus we could only estimate the frequency differences between each pair. The literature contains relatively precise values for the frequency difference between the transitions for each isotope. That is, there is data

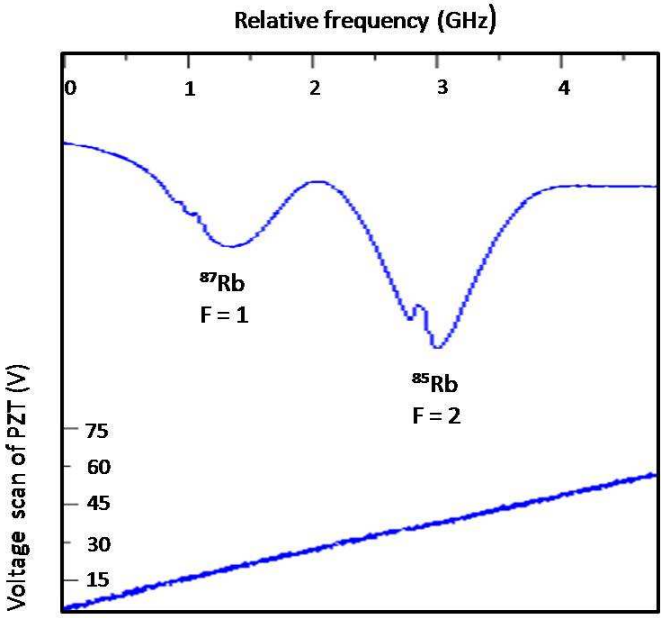

FIG. 11: Plot showing the ^{87}Rb, F = 1 and ^{85}, F = 2 absorption peaks together with the PZT scan (bottom). The relative frequency separation is estimated to be 1.9 GHz. Hyperfine features are also visible.

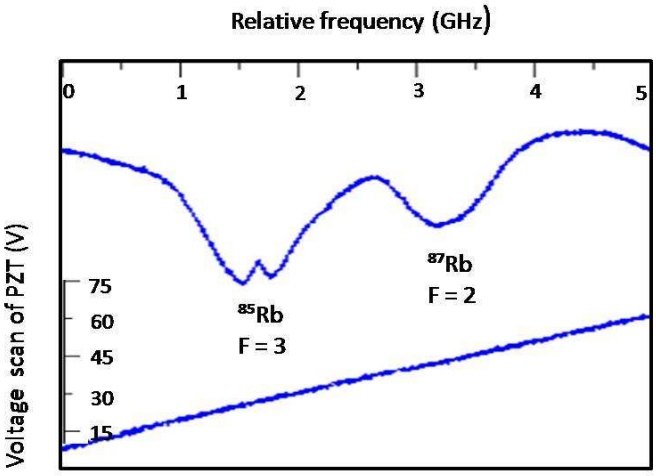

FIG. 12: The ^{85}Rb, F = 3 and ^{87}Rb, F = 2 absorption peaks with the PZT scan. We estimated a frequency seperation of 2.2 GHz based on the manufacturer's specifications of the change of length per volt for the PZT.

available in [13] that gives the frequency difference between the two peaks corresponding to ^{87}Rb and the two peaks corresponding to ^{87}Rb. We, on the other hand, could only quantitatively analyze the frequency differences between peaks corresponding to ^{87}Rb, $F = 1$ and ^{85}Rb, $F = 2$ as well as the peaks corresponding to ^{85}Rb, $F = 3$ and ^{87}Rb, $F = 2$. By using the value for $\frac{\Delta\nu_g}{V}$ calculated above, we estimated the frequency difference between the first two peaks (^{87}Rb, $F = 1$ and ^{85}Rb, $F = 2$) to be 1.9 GHz. Similarly, we estimated the frequency between the latter two peaks (^{85}Rb, $F = 3$ and ^{87}Rb, $F = 2$) to be 1.9 GHz. It should be noted that these are relatively coarse estimates, as we are merely utilizing the oscilloscope's grid to scale the frequency. According to [13], the frequency difference between the two resonance frequencies of ^{85}Rb is 3.036 Ghz, and the frequency difference between the two resonances of ^{87}Rb is 6.835 GHz. Utilizing one of the frequency differences reported in the literature, we can use our experimentally observed data to estimate the other. Specifically, the frequency difference between the two peaks corresponding to ^{87}Rb is the sum of the three frequency differences between consecutive peaks. Using our two observed frequency differences along with the reported value of the frequency difference between the two peaks corresponding to ^{85}Rb, we can estimate that the frequency difference between the two ^{87}Rb peaks is 1.9 GHz + 3.0 GHz + 1.9 GHz = 6.8 GHz, which is a reasonable estimate.

CONCLUSION

We found that a home-built ECDL system is sufficient to obtain the resonances of rubidium at 780 nm. Provided the appropriate controls over temperature, injection current, grating angle, and cavity length, the wavelength can be tuned within a standard deviation 0.08 pm, which is sufficient to produce spectra of the Rb vapor. An essential component of such a tuning system is a high-resolution wavelength measuring device, in our case provided by a wavemeter that uses Michelson interforometry concepts to measure the wavelength of coherent light to a tenth of a picometer. More surprisingly, we discovered that a rubidium cell with highly parallel windows can induce saturation spectroscopy despite Doppler broadening effects. In our experiment, the reflection of the first beam off the cell windows served as a pump beam to resolve hyperfine features within the absorption peaks. These assisted in correlating each feature with the known atomic transitions of rubidium. Mode hopping was a significant factor in our experiment. A mode hop within the range of the PZT scan meant that only two out of the four absorption peaks could be observed in a single scan. With slight adjustments to the injection current we could toggle between adjacent lasing modes to resolve the opposite two peaks. Ideally however, we should be able to view all four peaks in a single PZT scan. The elimination of mode hops would be an important future step for further experimentation. Additionally, it would be beneficial to correlate the hyperfine structures we resolved to the spin orbit coupling transitions of rubidium.